Article:
Zhao, S., Peng, Q., Du, D. et al. (2026) Enhancing safety of lithium-ion batteries in sustainable energy systems through intelligent minor short-circuits fault detection. Renewable and Sustainable Energy Reviews, 229. 116576. ISSN: 1364-0321

https://doi.org/10.1016/j.rser.2025.116576

Enhancing safety of lithium-ion batteries in sustainable energy systems through intelligent minor short-circuits fault detection

Shiwen Zhao[a], Qiao Peng[b], Dajun Du[c], Minrui Fei[c], Chen Peng[c], Heng Li[d], Yue Wu[d], Kang Li[e], Kailong Liu[a*]

[a] *School of Control Science and Engineering, Shandong University, Jinan 250100, Shandong, China*
[b] *Information Technology, Analytics & Operations Group, Queen's University Belfast, Belfast BT71NN, UK*
[c] *Shanghai Key Laboratory of Power Station Automation Technology, School of Mechatronics Engineering and Automation, Shanghai University, Shanghai, China*
[d] *School of Electronic Information, Central South University, Changsha 410083, Hunan, China*
[e] *School of Electronic and Electrical Engineering, University of Leeds, Leeds, LS2 9JT, UK*
[*]Corresponding author.
E-mail address: Kailong.Liu@email.sdu.edu.cn; kliu02@qub.ac.uk (K. Liu)

Abstract: The rapid growth of renewable energy integration and electric mobility has increased the demand for safe and reliable lithium-ion batteries, which are essential due to their high energy density, long lifespan, and efficiency. However, complex internal electrochemical reactions and external operational stress can induce minor short circuits (MSC) that are difficult to detect at early stages yet may escalate to thermal runaway, posing significant risks to large-scale energy storage systems. To address this challenge, this study proposes an unsupervised MSC fault diagnosis framework that integrates a hybrid feature extraction strategy with a deep support vector data description algorithm. The method employs two-dimensional correlation coefficients and two-dimensional wavelet transform to capture voltage consistency across cells and detect transient anomalies associated with fault development. These complementary features are fused into a multidimensional representation and processed by the deep model, which learns compact patterns of normal operating states and constructs a hypersphere for anomaly detection. The framework is validated using a laboratory module with six battery cells, demonstrating effective fault identification under varying operating conditions, fault severities, and battery chemistries, achieving a 94% fault detection rate with a 3% false alarm rate. Furthermore, the computational procedure relies on matrix-based feature construction and a lightweight feed-forward inference process, offering computational efficiency suitable for real-time deployment in battery management systems. Benefiting from its unsupervised and data-driven design, the framework exhibits strong generalizability under

diverse conditions and provides a promising pathway for enhancing the safety and reliability of future energy storage applications.

Key words: Lithium-ion battery, Short-circuit, Fault diagnosis, Unsupervised learning, Battery management.

1. Introduction

The depletion of fossil fuels and the urgent need to curb environmental pollution have significantly accelerated the global transition toward renewable energy sources [1,2]. However, the inherent intermittency and variability of renewables, such as solar and wind, present considerable challenges to maintaining grid stability and ensuring energy reliability [3,4]. To address this, efficient and scalable energy storage solutions are essential [5,6]. Among various technologies, lithium-ion batteries (LIBs) have emerged as a leading choice due to their high energy density, long cycle life, excellent efficiency, fast response, and low self-discharge rates [7,8]. These advantages make LIBs indispensable across a wide range of applications, including consumer electronics [9], electric vehicles [10], and increasingly, in large-scale stationary energy storage systems for load leveling, frequency regulation, and emergency backup [11,12]. As the demand for clean and flexible energy continues to grow, LIBs are playing an ever more critical role in enabling the development of a resilient, low-carbon energy infrastructure [13,14]. However, safety incidents caused by LIB failures have occurred with increasing frequency worldwide, raising serious concerns about their operational safety [15]. LIBs are susceptible to manufacturing defects, mechanical damage, and temperature fluctuations, and these factors can lead to various types of failures. In severe cases, such failures may trigger thermal runaway, creating significant risks to the safety and stability of the entire battery system [16,17]. Fault diagnosis technology plays a critical role by detecting early signs of failure before they escalate, allowing timely intervention to prevent catastrophic consequences [18]. Therefore, the development of accurate and timely fault diagnosis methods is essential to ensure the safety and reliability of LIBs, and to support their broader adoption in next-generation energy systems [19,20].

Faults in LIBs mainly include connection issues, short circuits, overcharge/over-discharge and sensor failures [21,22]. Among these, short-circuit faults are not only among the most prevalent but also represent a significant safety risk, contributing to a large proportion of battery-related incidents [23,24]. It is typically induced by manufacturing defects (e.g., metal impurities, diaphragm damage), material aging (e.g., lithium dendrite formation), mechanical damage (e.g., extrusion, puncture), environmental factors (e.g., high temperature,

humidity), or failures in the battery management system [25,26]. These issues may lead to unintended contact between the positive and negative electrodes, resulting in a short circuit. Such failures progress through multiple stages, initially presenting only subtle electrical or thermal anomalies, which makes early detection highly challenging [27]. As the fault worsens, however, it may initiate a rapid exothermic chain reaction, causing a steep temperature rise that can eventually lead to thermal runaway [28]. Consequently, the early identification of minor short-circuit (MSC) faults is essential for maintaining LIB safety [29,30]. Yet, the diagnosis of MSC faults is hindered by the complex, nonlinear behavior of LIBs and the concealed, progressive, and propagative nature of such faults, making timely and accurate detection highly challenging [31,32].

At present, short-circuit fault diagnosis methods are generally classified into three types: threshold-based, model-based, and data-driven approaches [33,34]. Threshold-based techniques detect faults by monitoring whether certain battery parameters exceed predefined limits [35]. For instance, Xia et al. [36] developed an adaptive threshold-based method capable of identifying faults such as overvoltage and overcurrent. Owing to its straightforward implementation and reliability, this approach has been widely adopted in battery management systems (BMS). However, it falls short in detecting early-stage MSC faults, as the associated parameter deviations are often too subtle to surpass the preset thresholds [37].

Model-based battery fault diagnosis methods typically construct battery models to predict real-time battery behavior and compare the model outputs with actual measurements [38]. A fault is indicated when the residual between them exceeds a predefined threshold [39,40]. Equivalent circuit models—such as Thevenin, RC, and dual polarization models—are widely used in battery applications [41,42]. For instance, Zheng et al. [43] proposed a quantitative diagnosis method for single lithium-ion cells, in which a first-order RC equivalent circuit model was constructed to estimate battery capacity. By analyzing the capacity differences of a short-circuited cell during charge–discharge cycles, this method enables quantitative fault diagnosis, but it is time-consuming and often requires several hours to complete the detection process. Xu et al. [44] designed a nonlinear H_∞ observer using an extended state-space model to estimate the state of charge (SOC) of LIBs. Short-circuit faults were detected by evaluating the discrepancy between the estimated and actual SOC values. The method based on this type of model has a simple structure and strong real-time performance, but is sensitive to battery aging and operating environment, and its diagnostic performance is limited by the accuracy of the model [45]. In addition,

electrochemical models have been applied to short-circuit fault diagnosis. Compared with conventional equivalent circuit models, they offer higher accuracy and therefore enable more precise fault detection. [46]. For example, Ma et al. [47] developed a simplified electrochemical model based on the pseudo-two-dimensional (P2D) framework and demonstrated that the predicted apparent diffusion coefficient can serve as a highly sensitive indicator of ISC during battery aging. The accuracy of this type of method has been effectively improved, but it has the disadvantages of complex modeling, high computational cost, and difficulty in real-time application [48,49].

With the progress of data science, numerous data-driven approaches employing signal processing and machine learning techniques have been developed for detecting battery short-circuit faults [50,51]. Unlike model-based methods, these approaches do not require an accurate mathematical model of the battery, but instead identify faults by analyzing measured data patterns [52]. Signal processing techniques typically extract fault-related features—such as entropy or correlation coefficients—from operational data and detect anomalies by comparing these features with reference values obtained under normal conditions [53,54]. For instance, Wu et al. [55] proposed a short-circuit fault diagnosis method based on voltage cosine similarity. This approach constructs a two-dimensional feature vector using battery voltage and current, and introduces a gain factor incorporating excitation information to further process the feature vector, thereby enhancing the separation and identification of fault. Li et al. [56] proposed an early ISC fault diagnosis method based on multivariate multiscale sample entropy (MMSE). This approach extracts fault-related features from multiple signals, including voltage, current and temperature, using MMSE to indicate the onset of faults. Although multiple signals are incorporated, no substantial improvement in detection accuracy or speed has been achieved. In addition, signal decomposition techniques such as empirical mode decomposition and wavelet transform have also been employed to extract fault features for fault detection. For example, Jiang et al. [57] employed wavelet packet decomposition to divide the original voltage signal into low- and high-frequency components, thereby facilitating the extraction of fault features. In general, such techniques are primarily employed as auxiliary tools for feature extraction and are rarely used independently for fault detection. In summary, signal-processing-based methods are simple and easy to implement, but their diagnostic accuracy is limited because they cannot effectively capture the nonlinear characteristics of batteries, and their performance often degrades significantly in the presence of noise.

Artificial intelligence (AI) has rapidly advanced in recent years, providing a suite of data-driven tools capable of extracting complex patterns and supporting intelligent decision-making in engineering systems [58,59]. Within this broader AI landscape, machine learning techniques offer powerful nonlinear mapping capabilities and have demonstrated considerable potential in battery fault diagnosis [60,61]. Depending on the training paradigm and the requirement for labeled data, these techniques can be broadly categorized into supervised and unsupervised learning [62]. Supervised learning methods typically rely on large, well-labeled fault datasets to train models that learn and recognize failure patterns, thereby enabling accurate and reliable diagnostic outcomes. [63,64]. For instance, Qiao et al. [65] proposed a machine learning-based internal short-circuit diagnosis method that segments voltage curves via the incremental capacity curve and applies dynamic time warping (DTW) to measure inter-cell similarity. Four statistical features of the DTW results are extracted and used to train a gradient boosting decision tree (GBDT) model, enabling accurate early ISC fault detection and localization under diverse operating conditions using only partial voltage data. However, its reliance on extensive fault data and the requirement for long-term test sequences for feature extraction significantly limit its practicality. In addition, recent advancements in deep learning techniques, such as convolutional neural networks (CNNs) and recurrent neural networks (RNNs), have gained widespread attention and have also been applied to short-circuit fault diagnosis [66,67]. For example, Cui et al. [68] proposed a rapid and accurate ISC detection method by integrating electrochemical impedance spectroscopy (EIS) with deep neural networks (DNNs), enabling reliable identification of ISC faults. However, it also faces the problem of scarce fault datasets, which raises doubts about the model's generalization ability. In summary, supervised learning methods have shown great potential in improving the accuracy of battery short-circuit fault diagnosis [69]. However, key challenges remain: the scarcity and difficulty of obtaining fault data lead to insufficient training samples for machine learning models, which greatly limits their effectiveness in practical fault diagnosis applications.

In contrast, unsupervised learning methods, which do not rely on labeled fault data and instead learn intrinsic patterns from normal operating conditions, offer a promising pathway to address the data scarcity and generalization issues faced by supervised approaches [70,71]. For example, Zhang et al. [72] proposed an early battery pack fault detection method that constructs a generalized dimensionless index with a tolerance factor, maps anomaly evolution into a two-dimensional space, and applies the LOF method with a differential strategy to accurately identify faulty batteries using real electric vehicle data. The method detects faults by capturing

inherent abnormal patterns without requiring labeled training data, thereby avoiding dependence on scarce fault samples. However, as an unsupervised method based on local density, LOF is sensitive to noise, which can distort density estimates and lead to false positives or negatives [73]. Support vector data description (SVDD) has also been applied to battery fault diagnosis. It constructs a compact and robust boundary using only normal samples, enabling accurate anomaly detection. By incorporating soft boundaries and regularization, SVDD reduces the impact of noise, providing a degree of anti-interference capability [74]. However, its reliance on predefined kernel functions and limited feature extraction can reduce effectiveness when handling complex or high-dimensional data, such as highly nonlinear LIB systems.

Based on the above analysis, accurately diagnosing early-stage MSC faults remains a significant challenge. To address this, this study introduces a novel fault diagnosis method for LIBs that integrates minor fault feature extraction with a deep SVDD algorithm. Specifically, voltage data are processed using two-dimensional correlation coefficients and two-dimensional wavelet transforms to extract fault features, which are then fed into the deep SVDD model for MSC fault detection. The main contributions of this study are as follows:

(1). To enhance the identification of subtle MSC fault features, a novel and effective hybrid feature extraction method is proposed. Initially, two-dimensional correlation coefficients are employed to capture correlation features from the battery voltage and its first-order difference. Subsequently, a mutation feature extraction approach based on two-dimensional wavelet transform is introduced to detect abrupt changes associated with fault onset. This combined method enables a more comprehensive representation of MSC fault characteristics.

(2). A deep SVDD algorithm is developed, leveraging the nonlinear fitting capabilities of deep learning to effectively extract complex nonlinear patterns from battery data, thereby enabling accurate MSC fault detection. Notably, the algorithm operates in an unsupervised manner and does not require fault data for training.

(3). Extensive experiments under varying operating conditions and fault severities are conducted to validate the robustness and generalization capability of the proposed method.

The rest of the paper is organized as follows. Section 2 provides a detailed description of the proposed MSC fault diagnosis framework based on the deep support vector description algorithm. Section 3 outlines the experimental platform and procedures. Section 4 presents the validation of the proposed framework using experimental data and discusses the corresponding results. Finally, Section 5 summarizes the research findings of this study.

2. Fault diagnosis scheme

In this section, the proposed combined minor fault feature extraction method is introduced, followed by a detailed explanation of the deep support vector description algorithm. Finally, the overall framework of the MSC fault diagnosis strategy for LIBs is presented.

2.1 Minor fault feature extraction

Short circuits are common in LIBs and often cause changes in voltage, current, and temperature. However, surface temperature responds slowly, and series-connected cells share the same current, making these parameters less effective for fault diagnosis. In contrast, voltage is easy to acquire and carries rich fault-related information [75]. Therefore, this study designed the following two feature extraction methods based on the characteristics of voltage data to extract key MSC fault features.

1) Two-dimensional correlation coefficient: The correlation coefficient is a statistical measure that quantifies the relationship between two variables. Unlike conventional approaches that rely solely on battery voltage, the proposed two-dimensional correlation coefficient integrates both the voltage and its first-order difference, enabling the extraction of more comprehensive fault characteristics., which is summarized as follows. Suppose there is a voltage sequence of length N:

$$V^j = \left[V_1^j, \dots, V_i^j, \dots, V_N^j\right] \tag{1}$$

where V_i^j represents the voltage of cell j at the i-th moment. Taking the first-order differences of the voltages and combining them gives:

$$P_i^j = \left[V_i^j, \frac{dV_i^j}{dt_i}\right] \approx \left[V_i^j, \frac{\Delta V_i^j}{\Delta t_i}\right] = \left[V_i^j, \frac{V_i^j - V_{i-1}^j}{t_i - t_{i-1}}\right] \tag{2}$$

where P_i^j is the voltage and its differential combination point corresponding to the i-th sampling point of the j-th cell, t_i is the i-th sampling moment. The P_i^j at each moment is combined to get:

$$P^j = \left[P_1^j, \ldots, P_i^j, \ldots, P_N^j\right] \tag{3}$$

The two-dimensional correlation coefficient between P^a and P^b is defined as follows. Calculate the mean of the two matrices P^a and P^b:

$$\overline{P^a} = \frac{1}{2k}\left(\sum_{i=1}^{k} V_i^a + \sum_{i=1}^{k} \frac{dV_i^a}{dt_i}\right) \tag{4}$$

$$\overline{P^b} = \frac{1}{2k}\left(\sum_{i=1}^{k} V_i^b + \sum_{i=1}^{k} \frac{dV_i^b}{dt_i}\right) \tag{5}$$

Then, the covariance of the two matrices is:

$$Cov(P^a, P^b) = \sum_{i=1}^{k}(V_i^a - \overline{P^a})(V_i^b - \overline{P^b}) + \sum_{i=1}^{k}\left(\frac{dV_i^a}{dt_i} - \overline{P^a}\right)\left(\frac{dV_i^b}{dt_i} - \overline{P^b}\right) \tag{6}$$

Next, calculate the standard deviation of each matrix:

$$\sigma_{P^a} = \sqrt{\sum_{i=1}^{k}(V_i^a - \overline{P^a})^2 + \sum_{i=1}^{k}\left(\frac{dV_i^a}{dt_i} - \overline{P^a}\right)^2} \tag{7}$$

$$\sigma_{P^b} = \sqrt{\sum_{i=1}^{k}(V_i^b - \overline{P^b})^2 + \sum_{i=1}^{k}\left(\frac{dV_i^b}{dt_i} - \overline{P^b}\right)^2} \tag{8}$$

Finally, the two-dimensional correlation coefficient between P^a and P^b is obtained:

$$TCC(a,b) = \frac{Cov(P^a, P^b)}{\sigma_{Pa}\sigma_{Pb}} \tag{9}$$

When using the two-dimensional correlation coefficient for feature extraction, the data sequence of each individual battery is compared with the corresponding average sequence derived from the entire battery pack. This comparison enables the extraction of features that reflect deviations from the overall behavior, thereby enhancing the sensitivity to subtle fault-related anomalies.

2) Feature extraction method based on two-dimensional wavelet transform: Two-dimensional wavelet transform is a technique used to decompose images or two-dimensional signals across spatial and frequency domains. It enables the extraction of features at multiple scales and orientations, and is widely applied in areas

such as image compression, edge detection, and related fields [76]. In this study, it is introduced into battery fault analysis to effectively extract abrupt features associated with fault occurrence, providing a more detailed representation of the transient characteristics during failure events. The basic principle of two-dimensional wavelet transform is as follows. The two voltage sequences V^1 and V^2 are combined into a two-dimensional matrix:

$$X = \begin{bmatrix} V_1^1 & \cdots & V_N^1 \\ V_1^2 & \cdots & V_N^2 \end{bmatrix} \tag{10}$$

Select a set of orthogonal discrete wavelet filters: low-pass filter $h[n]$, high-pass filter $g[n]$, $n = 0, 1, \ldots, L-1$. For each row $X_{i,:}$ convolution and downsampling operations are performed to obtain the decomposed low-frequency and high-frequency parts:

Low-frequency part: $$A_i[k] = \sum_{n=0}^{L-1} X_{i,n} * h[2k-n] \tag{11}$$

High-frequency part: $$D_i[k] = \sum_{n=0}^{L-1} X_{i,n} * g[2k-n] \tag{12}$$

where $A_i[k]$ is the low-frequency coefficient at the k-th position of the i-th row of the matrix, $D_i[k]$ is the high-frequency coefficient at the k-th position of the i-th row of the matrix. Combine the decomposed components of each row according to high and low frequencies to obtain two intermediate matrices: The matrix X_L consists of two rows of low-frequency components and the matrix X_H consists of two rows of high-frequency components. Then repeat similar convolution and down-sampling operations on each column of matrices X_L and X_H to obtain the final decomposition components of the two-dimensional wavelet transform:

$$DWT2(X) = \{LL, LH, HL, HH\} \tag{13}$$

where LL, LH, HL, HH are all decomposed subbands, and are all two-dimensional matrices. In this work, the two-dimensional discrete wavelet transform is implemented using the Daubechies-4 (db4) wavelet as the mother wavelet. The db4 wavelet offers suitable smoothness and compact support, making it effective for capturing localized fluctuations and multiscale features in battery data. A single-level decomposition is adopted to obtain the approximation and detail components, which provides adequate multi-resolution representation while avoiding unnecessary computational complexity. All analyses are conducted under this fixed wavelet configuration to ensure consistency and reproducibility. The LL component represents the low-frequency subband,

capturing the main contour and overall structure of the signal. The LH component corresponds to horizontal details, reflecting edge information along the horizontal axis, which in the context of voltage sequences, indicates abrupt changes over time. The HL component captures vertical details, highlighting edge information along the vertical axis, and corresponds to voltage anomalies across different cells. The HH component represents diagonal details, primarily associated with high-frequency noise within the two-dimensional signal. Considering that abrupt voltage variations exhibit strong sensitivity to micro-short-circuit faults in both temporal and spatial dimensions, this study focuses on the LH and HL components for feature extraction. The LH component characterizes edge variations along the time axis and effectively captures transient voltage fluctuations induced by micro-short circuits. The HL component reflects inter-cell spatial differences and can reveal abnormal voltage patterns resulting from uneven short-circuit pathways. In contrast, the HH component primarily represents high-frequency noise in the two-dimensional signal, corresponding to transient disturbances and random measurement errors. Its physical interpretability is limited, and its contribution to micro-short-circuit detection is relatively weak. The specific feature extraction formula is as follows:

$$MS(X) = SUM(LH \odot HL) \tag{14}$$

where $\odot$ represents the Hadamard (element-by-element) product of each matrix element, and SUM sums all the elements of the matrix.

2.2 Deep supports vector data description

SVDD is a one-class classification algorithm that constructs a minimum-volume hypersphere in feature space to enclose most normal samples, enabling the detection of anomalies outside the sphere. With strong generalization ability, it is suitable for tasks with unknown data distributions or limited to normal samples [77]. However, SVDD's dependence on predefined kernels and limited feature extraction makes it less effective for complex or high-dimensional data, such as highly nonlinear LIB systems. To address these limitations, this study employs a deep SVDD approach. As illustrated in Fig. 1, a neural network is utilized to learn end-to-end feature mappings, enabling the construction of a more precise hypersphere that encloses normal samples in a high-dimensional space. This enhances both the accuracy and robustness of battery fault detection. The detailed principle is as follows. Deep SVDD uses a fully connected neural network to map normal data samples to a high-dimensional feature space and learn a minimum volume hypersphere centered at a predefined point [78]. The training goal is to

minimize the average distance between the mapped features and the center while regularizing the network parameters. The corresponding loss function is defined as follows:

$$L(W) = \frac{1}{N}\sum_{i=1}^{S}\left\|\varphi(\tilde{X}_i; W) - c\right\|^2 + \frac{\lambda}{2}\|W\|^2 \tag{15}$$

where S is the number of sample sets, $\tilde{X}_i$ is the i-th sample, i.e., the standardized feature vector, W is the neural network learning parameter, c is the center of the hypersphere, initialized to the mean of all outputs, $\varphi(.;W)$ is the characteristic representation of the neural network parameters, and λ is the regularization term coefficient; the first term uses a quadratic loss function, the goal is to penalize the Euclidean distance from all points in the space to the center of the sphere c, and the second term is a regularization term to prevent the network from overfitting. This is a deep SVDD hard boundary model based on the assumption that the training data is completely noise-free, which shrinks the hypersphere by minimizing the average distance from all data representations to the center of the sphere.

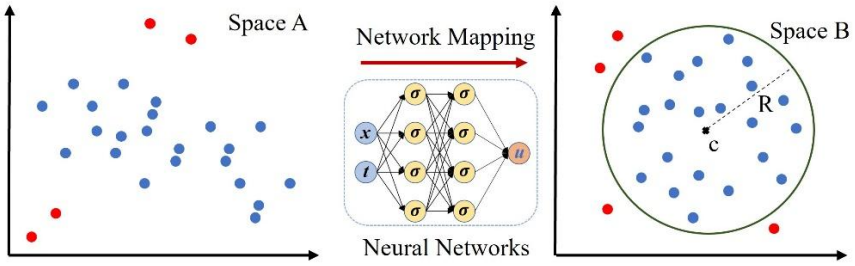

Fig. 1. Schematic diagram of the deep SVDD algorithm.

In actual data, soft-boundary deep SVDD shrinks the hypersphere by penalizing the radius R of the hypersphere and the data falling outside the hypersphere. The formula of the soft-boundary deep SVDD target is as follows:

$$L_a(W) = R^2 + \frac{1}{\nu N}\sum_{i=1}^{S}\max\left\{\left\|\varphi(\tilde{X}_i; W) - c\right\|^2 - R^2\right\} + \frac{\lambda}{2}\|W\|^2 \tag{16}$$

In the formula, the first term minimizes R^2 to minimize the volume of the hypersphere; the second term is a penalty term for out-of-bounds points, and the hyperparameter $\nu \in (0,1]$ controls the trade-off between the volume of the sphere and out-of-bounds points; the third term is a regularization term to prevent the network from overfitting.

After training the model using normal samples, the neural network parameters W^* and trained hypersphere radius R^* that can describe the normal sample distribution can be obtained. Notably, the used network adopts a fully connected architecture with two hidden layers of sizes 100 and 50, respectively. Each layer uses the ReLU activation function to enhance nonlinear feature extraction while maintaining training stability. The center of the hypersphere c is initialized as the mean of all network outputs obtained from a forward pass using the normal training samples. The model is optimized using the Adam optimizer with a learning rate of 1×10^{-3}, and the training is performed for 100 epochs with a batch size of 64. These settings ensure stable convergence of the hypersphere and reliable representation of the distribution of normal samples. Input the sample to be tested $\tilde{X}_{test}$ into the model to obtain the anomaly score:

$$s(\tilde{X}_{test}) = \left\|\varphi(\tilde{X}_{test}; W^*) - c\right\|^2 - R^{*2} \tag{17}$$

Subsequently, the abnormal score obtained by evaluation can be used to complete the detection of battery MSC faults.

2.3 Framework for battery MSC diagnosis

Based on the above principle, accurate diagnosis of MSC faults in LIBs can be achieved by identifying subtle transient deviations from previously learned normal behavior, thereby enabling earlier detection before conventional safety thresholds are reached. The overall process of the proposed fault diagnosis framework is illustrated in the flowchart shown in Fig. 2. First, the voltage of each individual cell in the series-connected battery module is measured using voltage sensors and processed to obtain its first-order difference. To amplify transient time-edge variations and inter-cell spatial discrepancies that are highly sensitive to early micro-short-circuit behavior, correlation features are extracted using the two-dimensional correlation coefficient, and mutation-related features are further captured by the selected wavelet detail components (LH and HL). Finally, the extracted hybrid features from each cell are input into the proposed deep SVDD model, which is trained exclusively on normal operating data to learn a compact representation of normal dynamics. Deviations from this compact hypersphere are converted into anomaly scores, and sliding-window inference enables the system to flag abnormal patterns, such as minor transient spikes or subtle cell-to-cell inconsistencies, before cell voltage or temperature exceeds safety limits, thereby ensuring accurate identification and localization of MSC faults. In the subsequent

experimental part, the proposed method will be comprehensively validated under a wider range of conditions, including different temperatures, operating profiles, fault severities, cell chemistries, and aging states.

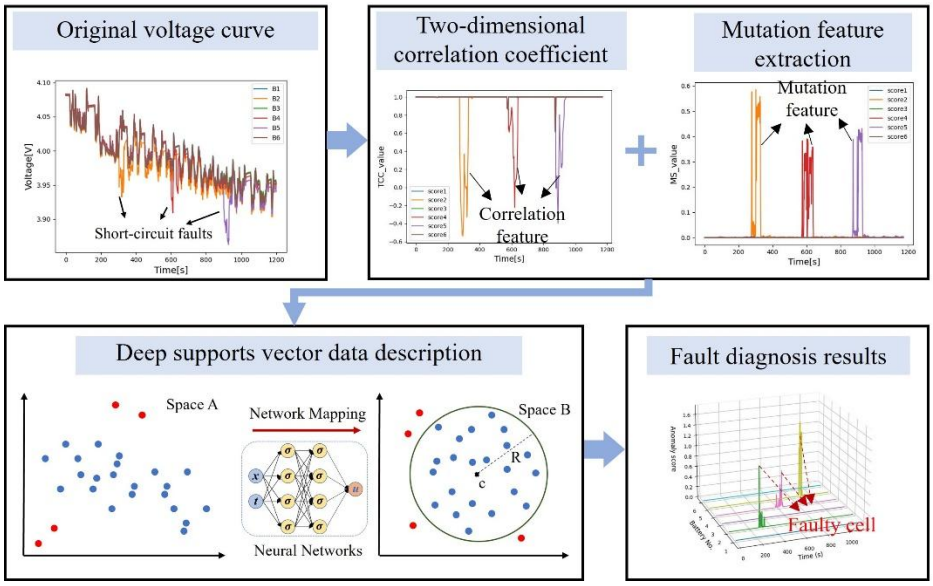

Fig. 2. Framework diagram of battery MSC fault diagnosis.

2.4 Performance metrics

To evaluate the performance of the proposed deep SVDD-based battery MSC fault diagnosis method, two metrics are employed: fault detection rate (FDR) and fault misdiagnosis rate (FMR):

$$FDR = \frac{\#\{I|f(I)=1 \cap D(I)=1\}}{\#\{I|f(I)=1\}} \times 100\% \tag{17}$$

$$FMR = \frac{\#\{I|f(I)=0 \cap D(I)=1\}}{\#\{I|f(I)=0\}} \times 100\% \tag{18}$$

where $\#\{x\}$ denotes the number of faults in the set x, $f(I) = 1$ denotes battery fault, $f(I) = 0$ denotes normal data, and $D(I) = 1$ indicates the detected fault.

3. Experiment

In order to verify the effectiveness and robustness of the proposed method, an experimental platform for battery short-circuit fault testing is established, as shown in Fig. 3. The platform comprises three main components: an Arbin battery tester for charge and discharge control, a temperature chamber for regulating the experimental environment, and a computer for data acquisition and processing. The experiment utilizes six ternary lithium-ion

(NCM) batteries ($Li(NiCoMn)O_2$), with their specific parameters detailed in Table 1. The experimental procedure is as follows: initially, the battery is charged to 4.1 V using a 1C constant current–constant voltage (CC-CV) charging protocol. After charging, the battery is allowed to rest for one hour. Subsequently, MSC faults are introduced to simulate the fault scenarios under the three operating conditions of urban dynamometer driving schedule (UDDS), new European driving cycle (NEDC) and federal urban driving schedule (FUDS) as shown in Fig. 4.

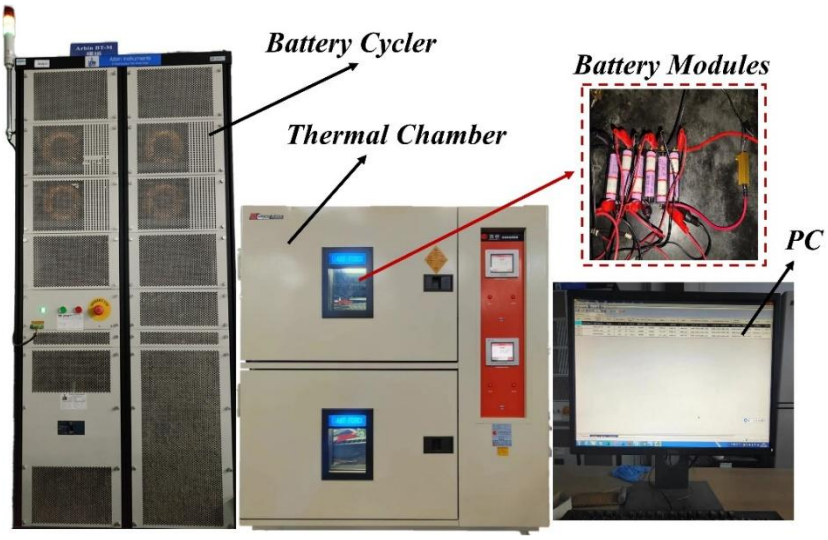

Fig. 3. Battery testing platform.

Table 1. Battery specifications.

Battery type	Nominal voltage	Nominal capacity	Charge cut-off voltage	Discharge cut-off voltage
INR18650-2P	3.7V	2Ah	4.2V	2.5V

Short-circuit faults are sequentially introduced into Cells 2, 4, and 5 during the experiment. Specifically, Cell 2 experience a 30 s short-circuit event at the 300 s mark. At the 600th s, Cell 4 is subjected to a 10 s short-circuit, followed by a 20 s recovery period, and then another 10 s short-circuit. Later, at the 900th s, Cell 5 encounter a 30 s short-circuit condition. It is worth noting that the resistance of the short-circuit resistor used in the tests—selected based on relevant literature—ranged from 1 Ω to 3 Ω [79].

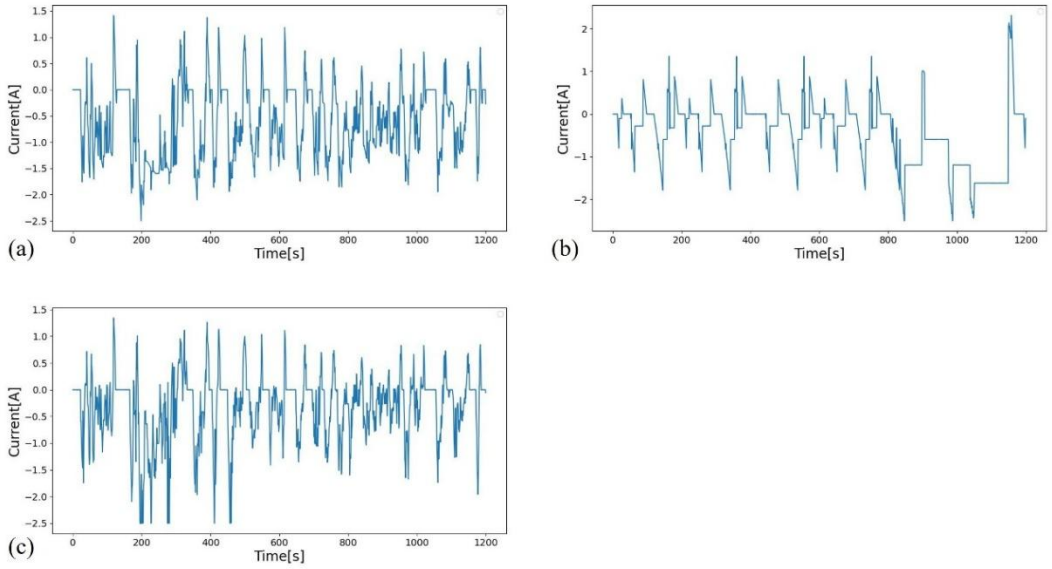

Fig. 4. Battery cycle test conditions. (a): Urban dynamometer driving schedule; (b): New European driving cycle; (c): Federal urban driving schedule.

4. Results and discussions

In this section, a set of fault experiments is carried out under diverse operating conditions and varying fault severities to verify the effectiveness, robustness, and generalization ability of the proposed method. Furthermore, comparative analyses with traditional fault diagnosis techniques are conducted to highlight the advantages of the proposed approach.

4.1 Verification of method effectiveness

The MSC fault diagnosis results of the proposed method under UDDS conditions are presented in Fig. 5. Specifically, Fig. 5(a) displays the voltage curves of individual cells during MSC fault events under UDDS operation. At around 300 s, cell 2 experienced a short-circuit fault lasting 30 s, leading to a voltage drop to approximately 3.93 V. Cell 4 encountered two short-circuit events at 600–610 s and 630–640 s, respectively, each causing voltage fluctuations of roughly 0.06 V. Meanwhile, cell 5 underwent a fault at 900 s, also lasting 30 seconds, with a maximum voltage drop close to 0.9 V. Notably, despite the voltage decreases in the affected cells, the values remained above the BMS cut-off threshold, meaning that no alarm would be triggered. As such, traditional threshold-based approaches are incapable of identifying these minor faults. Fig. 5(b) and 5(c) present the extracted fault features from each cell's voltage sequence using the proposed two-dimensional correlation

coefficient and two-dimensional wavelet transform methods, respectively. As shown, during MSC fault events, the two-dimensional correlation coefficient exhibits a sharp decline, while the mutation score rises significantly, indicating that the proposed feature extraction methods can effectively capture the fault characteristics. It is noteworthy that slight decreases in the two-dimensional correlation coefficient can also be observed in normal cells at around 570 s and 860 s, which are attributed to noise disturbances. Therefore, to enhance feature robustness and diagnostic reliability, the two-dimensional correlation coefficient should be used in conjunction with the wavelet transform-based method for comprehensive fault feature representation.

Fig. 5(d) presents the final fault diagnosis results obtained by processing the extracted features using the proposed deep SVDD method. As shown, abrupt increases in the anomaly score clearly correspond to the occurrence of minor faults. Importantly, during normal battery operation, the anomaly score remains consistently low, effectively avoiding false alarms. These results demonstrate that the proposed method can accurately detect MSC faults, even when the voltage does not exceed the predefined safety threshold. Notably, the proposed method is trained entirely offline using normal-operation data, so training does not affect real-time deployment. During operation, only a single forward pass of the Deep SVDD network and a distance calculation to the hypersphere center are required, resulting in very low computational load. The average inference time per sample is approximately 0.3–0.5 ms on a standard CPU, with memory usage below 5 MB, demonstrating that the approach meets real-time feasibility requirements for practical battery-management applications.

4.2 Fault diagnosis results under different working conditions

In real-world applications, LIBs operate under diverse and dynamic conditions, including varying current rates and load profiles. These fluctuations can significantly affect the battery's electrical behavior, such as voltage response and internal resistance, thereby altering fault features and increasing the difficulty of accurate fault diagnosis. To further evaluate the robustness and adaptability of the proposed method, this section presents the diagnostic results under NEDC and FUDS conditions.

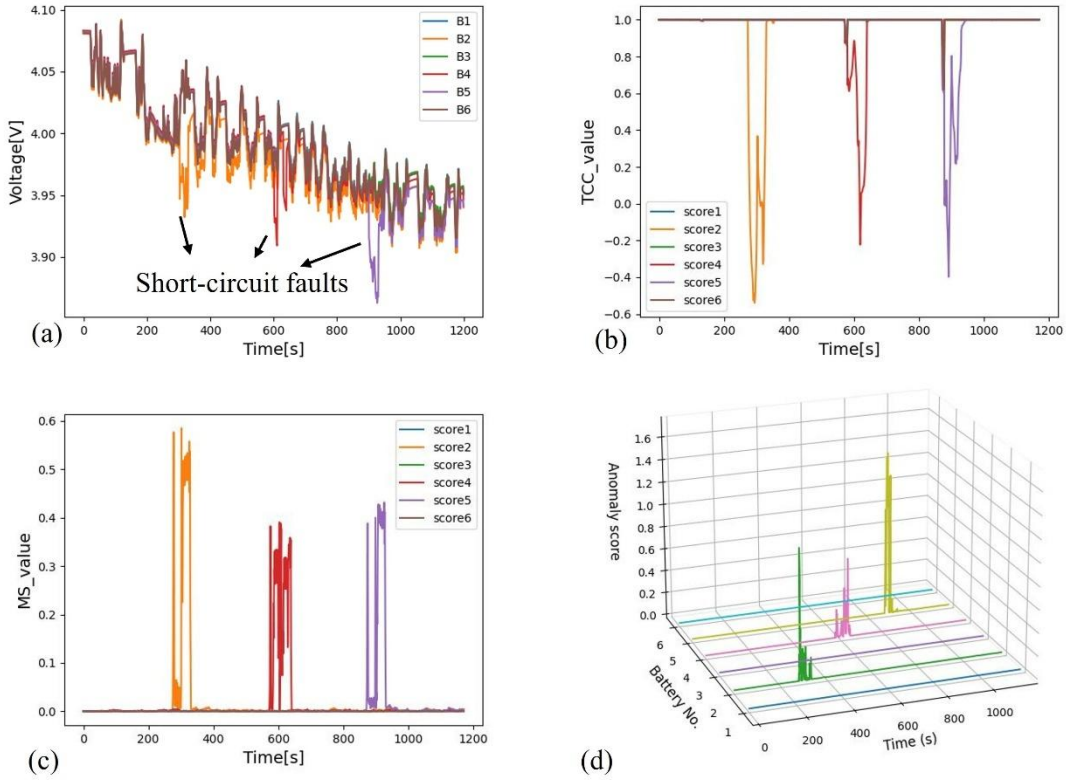

Fig. 5. Fault diagnosis results under UDDS conditions. (a): Battery voltage sequence data; (b): Extracted two-dimensional correlation coefficient fault features; (c): Fault mutation features extracted using two-dimensional wavelet transform; (d): Final fault detection result.

Fig. 6(a) and Fig. 6(c) illustrate the voltage sequences of the battery pack under NEDC and FUDC operating conditions, respectively. Under the NEDC profile, the voltage fluctuations exhibit a relatively smooth and regular pattern, which makes it easier to distinguish fault-induced deviations from normal behavior. In contrast, the FUDC condition imposes a more dynamic and complex load on the battery, resulting in frequent and abrupt voltage changes. These fluctuations often resemble the variations caused by MSC faults, making it significantly more challenging to isolate and identify fault signatures. This highlights the importance of robust diagnostic methods capable of handling complex and noisy operational environments. Fig. 6(b) displays the fault diagnosis results under NEDC operating conditions. It can be seen that the anomaly scores for the faulty cells (2, 4, and 5) remain consistently elevated, with average peak values around 0.5, which are markedly higher than those of the healthy cells, whose scores remain near 0.02. In Fig. 6(d), the diagnostic results under FUDS conditions are shown. Despite the increased complexity of the operating environment, the anomaly scores for the same faulty cells

exceed 0.6, while the maximum score for the normal cells remains around 0.07. These findings demonstrate that the proposed method maintains a clear distinction between normal and faulty conditions across different load profiles, indicating strong robustness and adaptability to varying operational scenarios.

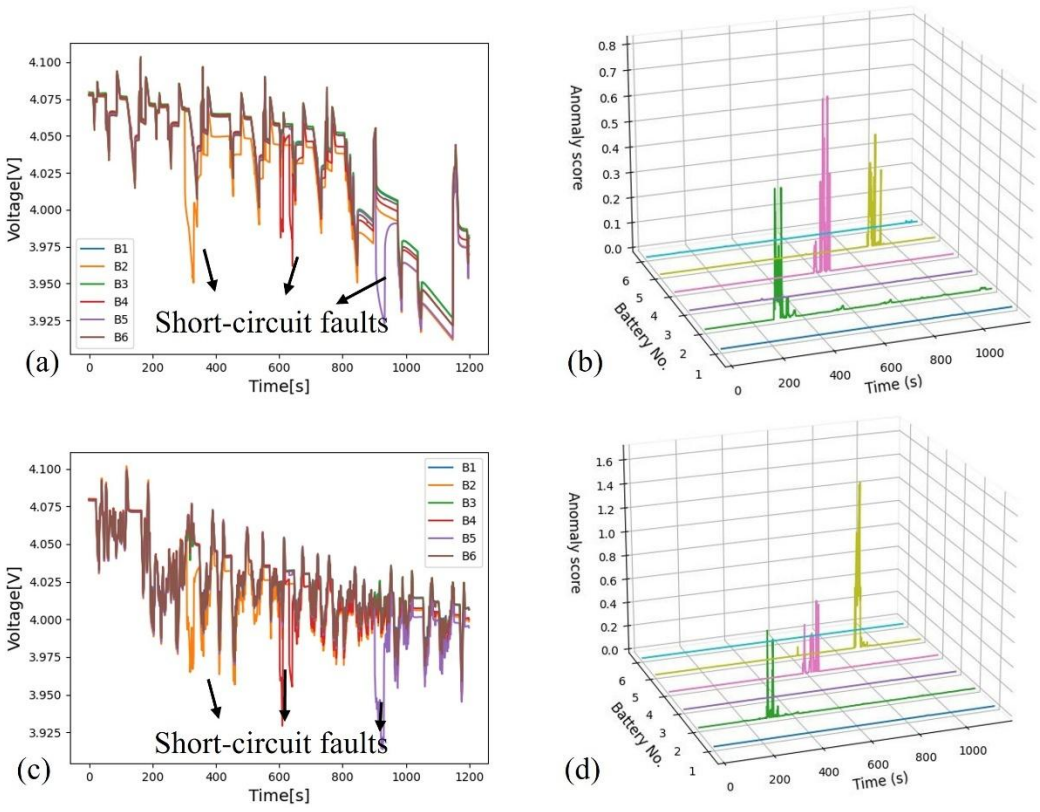

Fig. 6. Fault diagnosis results under different working conditions. (a): Battery voltage sequence data under NEDC conditions; (b): Fault detection result under NEDC conditions; (c): Battery voltage sequence data under FUDS conditions; (d): Fault detection result under FUDS conditions.

4.3 Fault diagnosis results at different fault levels

During normal battery operation, faults can arise unpredictably, with varying degrees of severity. In some cases, severe faults may develop even without noticeable early-stage voltage anomalies, posing a challenge for timely detection. To evaluate the generalization capability of the proposed method under diverse fault conditions, this section presents additional diagnostic results corresponding to two different levels of fault severity.

Fig. 7(a) and 7(c) depict the voltage sequences under external resistances of 2 Ω and 4 Ω, respectively. As the resistance increases, the severity of the short-circuit fault decreases due to reduced fault current. Specifically, at

2 Ω and 4 Ω, the maximum voltage drops observed during the fault events are approximately 0.07 V and 0.04 V, respectively. In contrast, a lower resistance results in a greater voltage deviation, indicating a more severe fault. This behavior is primarily caused by the current shunting effect of the short-circuit resistor. Importantly, the proposed method maintains stable diagnostic performance across different fault intensities and can reliably identify abnormal cells. As shown in Figs. 7(b) and 7(d), the anomaly score consistently captures the onset of faults at both fault levels. Although the anomaly score of cell 2 under the milder fault condition in Fig. 7(d) is relatively low and may increase the risk of misclassification, it remains clearly distinguishable from the normal cell behavior. These results confirm that the proposed method can effectively identify subtle MSC faults embedded in voltage sequences, even when such anomalies are undetectable using traditional threshold-based approaches.

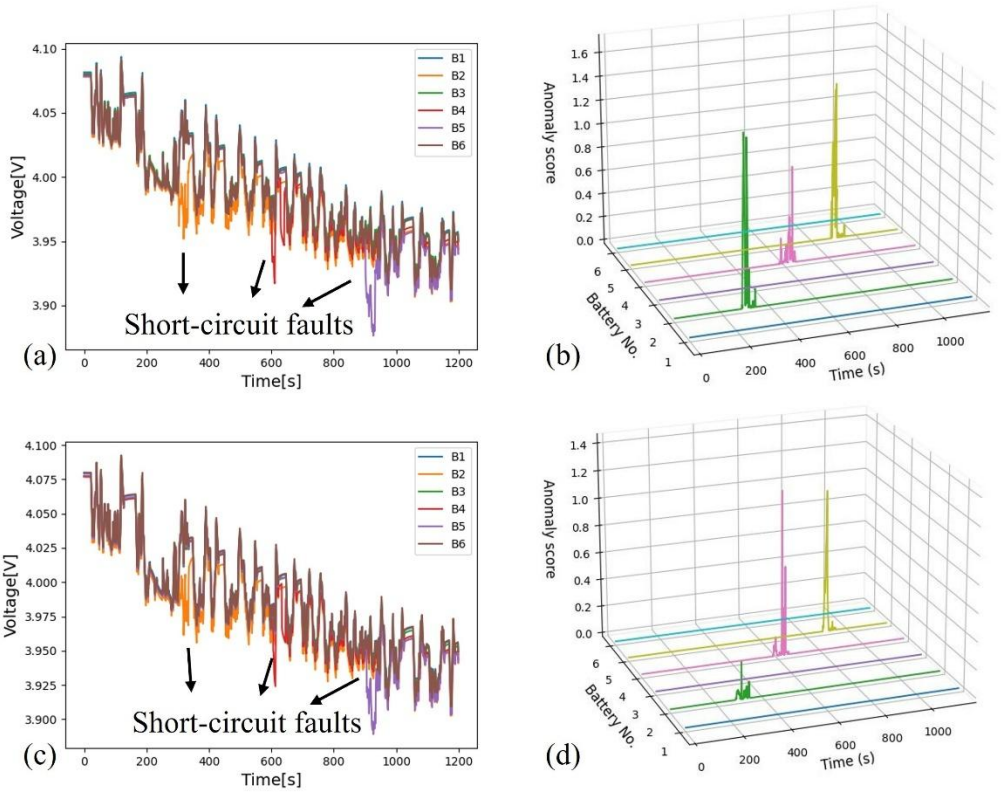

Fig. 7. Fault diagnosis results under different fault levels. (a): Battery voltage sequence data at resistance 2 Ω; (b): Fault detection result at resistance 2 Ω; (c): Battery voltage sequence data at resistance 4 Ω; (d): Fault detection result at resistance 4 Ω.

4.4 Fault diagnosis results under more comprehensive conditions

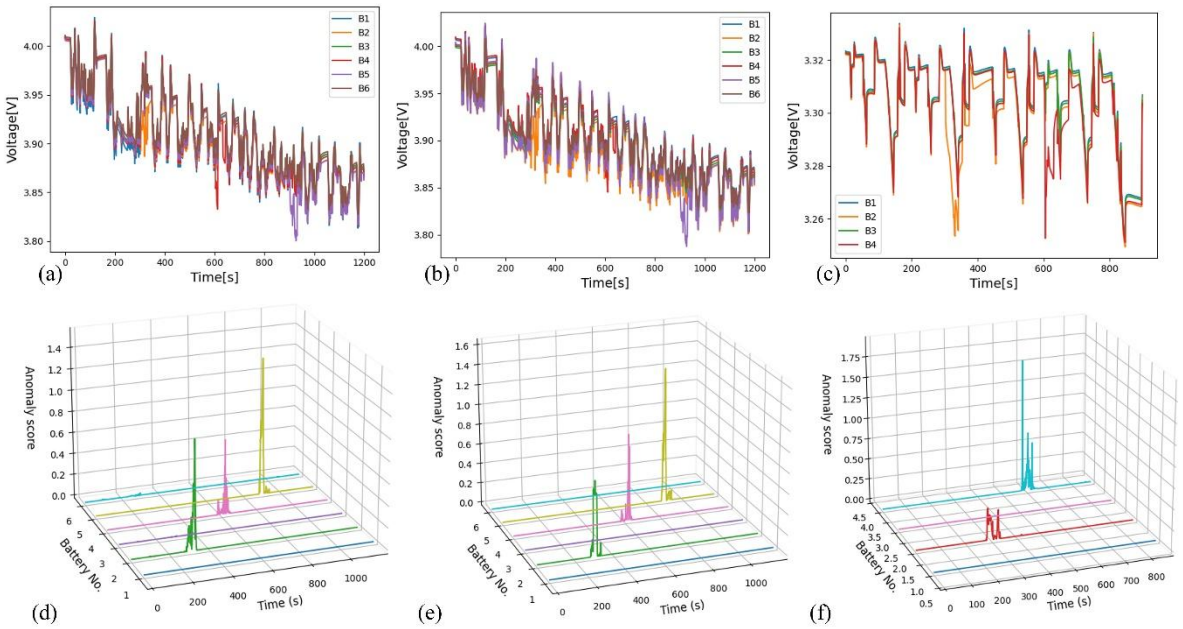

Fig. 8. Fault diagnosis results under more comprehensive conditions. (a): Battery voltage sequence data at 15℃; (b): Battery voltage sequence data under battery aging conditions; (c): Voltage sequence data of four 15Ah LFP cells; (d): Fault detection results at 15℃; (e): Fault detection results under battery aging conditions; (f): Fault detection results on LFP batteries.

To more comprehensively validate the effectiveness and generalizability of the proposed method, additional experiments are conducted under different battery chemistries (LFP), temperatures, and aging conditions. As shown in Fig.8, the proposed method maintains stable and reliable performance across all scenarios. Moderate temperature variations and aging-induced performance degradation exert limited influence on the manifestation of micro short-circuit faults, and the corresponding detection results further confirm the robustness of the proposed framework. It is worth noting that in Fig. 8(c), the LFP battery module experienced micro short-circuit events in cells 2 and 4 at 300 s and 600 s, respectively. The resulting voltage fluctuations were extremely subtle and closely resembled patterns observed during normal operation, thereby increasing the difficulty of fault identification. Nevertheless, the proposed method successfully detected these weak faults, demonstrating its sensitivity to small transient deviations and inter-cell inconsistencies. In summary, the results across different chemistries,

temperatures, and aging conditions verify that the proposed method remains stable, robust, and effective under a wide range of practical operating environments.

4.5 Comparison of the existing detection methods

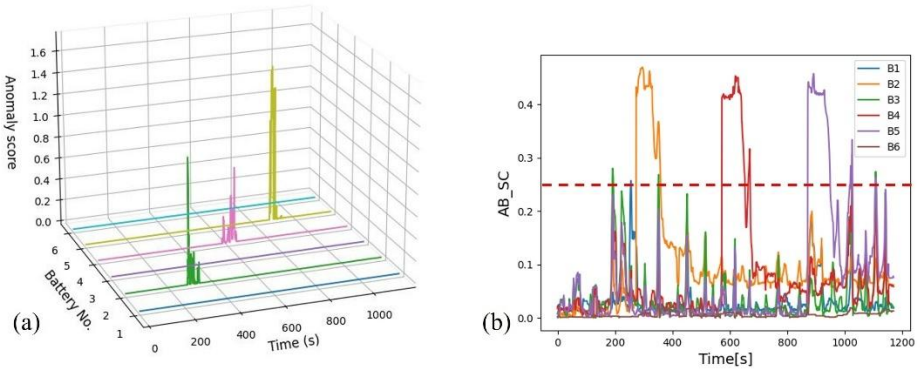

Fig. 9. Comparison of the diagnosis results between the proposed method and the isolation forest method. (a): Fault diagnosis results of the proposed method; (b): Fault diagnosis results of the isolation forest method.

To highlight the advantages of the proposed method, this paper compares it with three traditional fault diagnosis techniques, namely Isolation Forest, Sample Entropy, and Correlation Coefficient Detection, as well as a state-of-the-art deep learning approach, the Deep Autoencoder. For all comparison methods, faults are identified by applying predefined thresholds to their respective output metrics. For fairness and consistency, all methods are evaluated using the same test dataset, enabling a direct comparison of diagnostic accuracy and robustness under identical conditions. Fig. 9 shows the diagnosis results of the proposed method and the random forest method for MSC faults with a short-circuit resistance of 1.5 Ω under UDDS conditions. It is evident that the diagnostic method based on Isolation Forest struggles to effectively distinguish between normal and faulty conditions. The anomaly scores of normal cells remain relatively high and are close to those observed during fault occurrences, increasing the likelihood of false alarms. In contrast, the proposed method yields significantly lower anomaly scores for normal cells, while maintaining distinctly higher scores during fault events.

Table 2. Comparison of different methods for MSC fault detection.

	Sample entropy	Correlation coefficient	Isolation forest	Autoencoder	Proposed method
FDR	62%	75%	91%	92%	**94%**
FMR	34%	43%	15%	7%	**3%**

The comparison results of all methods are shown in Table 2. It can be observed that the autoencoder method significantly improves performance compared with the three traditional fault detection techniques, achieving an FDR of 92% and an FMR of 7%. This improvement primarily stems from the deep neural network architecture of the autoencoder, which enhances its ability to capture the nonlinear characteristics of LIBs. The proposed method further outperforms all the above techniques, achieving an FDR of 94% and an FMR of only 3%. These substantial gains demonstrate the strong capability of deep SVDD in modeling nonlinear data and effectively reducing false diagnoses.

5. Conclusion

Short-circuit failures pose a critical safety risk to LIBs, as they can trigger thermal runaway and significantly compromise the stable operation of renewable energy systems. To mitigate this risk, this study presents a novel MSC fault diagnosis approach for LIBs, which integrates a combined micro-fault feature extraction strategy with a deep SVDD-based detection algorithm. Based on extensive experimental validation, the following conclusions are drawn:

1. The proposed method enables effective real-time detection of MSC faults, even when cell voltages remain within the nominal safety range, by leveraging the designed feature set and the deep SVDD algorithm.

2. The method demonstrates strong robustness and generalization across varying operating profiles (UDDS, NEDC, and FUDS) and fault severities (1, 2, and 4 Ω), and additional validation using LFP batteries confirms that its diagnostic performance is consistent across the tested battery chemistries (NCM and LFP). Accordingly, the overly broad claim of “cross-chemistry compatibility” has been revised to reflect that generalization is supported only within the evaluated chemistries.

3. With a FDR of 94% and a FMR of only 3%, the proposed method outperforms conventional diagnostic techniques such as sample entropy, correlation coefficient analysis, and isolation forest, indicating superior accuracy and reliability.

Owing to its data-driven and unsupervised nature, the proposed framework demonstrates promising adaptability within the tested chemistries and operating scenarios, providing a foundation for improving early-stage fault intervention and enhancing the safety and reliability of energy storage systems. Future work will focus on

deploying the proposed diagnostic framework in real-time embedded systems within practical BMS platforms and evaluating its performance in large-scale battery modules, thereby further validating its applicability and robustness under real-world operating conditions.

Acknowledgements

This work was supported by the National Natural Science Foundation of China under Grant 62373224, and Shenzhen Science and Technology Program under Grant GJHZ20240218113404009, and Natural Science Foundation of Shandong Province under Grant ZR2024JQ021.

Reference

[1] Liu, K., Liu, Y., Peng, Q., Cui, N., & Zhang, C. (2025). Interpretable Data-Driven Learning with Fast Ultrasonic Detection for Battery Health Estimation. IEEE/CAA Journal of Automatica Sinica, 12(1), 267-269.

[2] Khoharo, H., Selvaraj, J., Hasanuzzaman, M., Kumar, L., & Manghwar, R. (2025). Global advancement, prospect and challenges of battery thermal management systems: A comprehensive review. Renewable and Sustainable Energy Reviews, 222, 115923.

[3] Anvari, S., Medina, A., Merchán, R. P., & Hernández, A. C. (2025). Sustainable solar/biomass/energy storage hybridization for enhanced renewable energy integration in multi-generation systems: A comprehensive review. Renewable and Sustainable Energy Reviews, 223, 115997.

[4] Ngoy, K. R., Lukong, V. T., Yoro, K. O., Makambo, J. B., Chukwuati, N. C., Ibegbulam, C., ... & Jen, T. C. (2025). Lithium-ion batteries and the future of sustainable energy: A comprehensive review. Renewable and Sustainable Energy Reviews, 223, 115971.

[5] Zhang, Z., Chen, Y., Ma, T., Tian, H., Liu, J., Zhou, M., & Wang, W. (2025). Multi-type energy storage expansion planning: A review for high-penetration renewable energy integration. Renewable and Sustainable Energy Reviews, 219, 115853.

[6] Liu, K., Ashwin, T. R., Hu, X., Lucu, M., & Widanage, W. D. (2020). An evaluation study of different modelling techniques for calendar ageing prediction of lithium-ion batteries. Renewable and Sustainable Energy Reviews, 131, 110017.

[7] Li, Y., Jiang, L., Zhang, N., Wei, Z., Mei, W., Duan, Q., ... & Wang, Q. (2024). Early warning method for thermal runaway of lithium-ion batteries under thermal abuse condition based on online electrochemical impedance monitoring. Journal of Energy Chemistry, 92, 74-86.

[8] Takyi-Aninakwa, P., Wang, S., Liu, G., Fernandez, C., Kang, W., & Song, Y. (2025). Deep learning framework designed for high-performance lithium-ion batteries state monitoring. Renewable and Sustainable Energy Reviews, 218, 115803.

[9] Xing, W. W., Zhang, Z., & Shah, A. A. (2025). Enhanced Gaussian process dynamical modeling for battery health status forecasting. Renewable and Sustainable Energy Reviews, 208, 115045.

[10] Khezri, R., Steen, D., Wikner, E., & Tuan, L. A. (2024). Optimal V2G scheduling of an EV with calendar and cycle aging of battery: An MILP approach. IEEE Transactions on Transportation Electrification, 10(4), 10497-10507.

[11] Liu, K., Liu, Y., Zhao, S., Li, X., & Peng, Q. (2024). An Ultrasonic Wave-Based Method for Efficient State-of-Health Estimation of Li-Ion Batteries. IEEE Transactions on Industrial Electronics.

[12] Liu, K., Wei, Z., Zhang, C., Shang, Y., Teodorescu, R., & Han, Q. L. (2022). Towards long lifetime battery: AI-based manufacturing and management. IEEE/CAA Journal of Automatica Sinica, 9(7), 1139-1165.

[13] Chen, S., Wei, X., Wu, H., Chen, K., Zhang, G., Wang, X., ... & Ouyang, M. (2025). Multi-functional thermal barrier suppresses battery thermal runaway propagation and degradation. Renewable and Sustainable Energy Reviews, 223, 116056.

[14] Guo, W., Yang, L., Deng, Z., Xiao, B., & Bian, X. (2023). Early diagnosis of battery faults through an unsupervised health scoring method for real-world applications. IEEE Transactions on Transportation Electrification, 10(2), 2521-2532.

[15] Shang, Y., Wang, S., Tang, N., Fu, Y., & Wang, K. (2024). Research progress in fault detection of battery systems: A review. Journal of Energy Storage, 98, 113079.

[16] Li, X., Gao, X., Zhang, Z., Chen, Q., & Wang, Z. (2023). Fault diagnosis and detection for battery system in real-world electric vehicles based on long-term feature outlier analysis. IEEE Transactions on Transportation Electrification, 10(1), 1668-1679.

[17] Hu, X., Zhang, K., Liu, K., Lin, X., Dey, S., & Onori, S. (2020). Advanced fault diagnosis for lithium-ion battery systems: A review of fault mechanisms, fault features, and diagnosis procedures. IEEE Industrial Electronics Magazine, 14(3), 65-91.

[18] Abdolrasol, M. G., Ayob, A., Lipu, M. H., Ansari, S., Kiong, T. S., Saad, M. H. M., ... & Kalam, A. (2024). Advanced data-driven fault diagnosis in lithium-ion battery management systems for electric vehicles: Progress, challenges, and future perspectives. ETransportation, 22, 100374.

[19] Tang, A., Wu, Z., Xu, Y., Liu, K., & Yu, Q. (2024). Cloud-Based Li-ion Battery Anomaly Detection, Localization and Classification. IEEE Transactions on Industrial Informatics.

[20] Machlev, R. (2024). EV battery fault diagnostics and prognostics using deep learning: Review, challenges & opportunities. Journal of Energy Storage, 83, 110614.

[21] Xiong, R., Sun, X., Meng, X., Shen, W., & Sun, F. (2024). Advancing fault diagnosis in next-generation smart battery with multidimensional sensors. Applied Energy, 364, 123202.

[22] Xu, Y., Ge, X., Guo, R., & Shen, W. (2025). Recent advances in model-based fault diagnosis for lithium-ion batteries: A comprehensive review. Renewable and Sustainable Energy Reviews, 207, 114922.

[23] Zhang, B., Chen, Z., Jiao, M., & Wang, K. (2025). Rapid diagnosis and assessment of lithium-ion battery short circuit in three seconds across a wide range of short-circuit resistances. Applied Energy, 390, 125872.

[24] Zhang, X., Yang, W., Yan, L., Kaleem, M. B., & Liu, W. (2024). Adaptive internal short-circuit fault detection for lithium-ion batteries of electric vehicles. Journal of Energy Storage, 84, 110874.

[25] An, Z., Shi, T., Du, X., An, X., Zhang, D., & Bai, J. (2024). Experimental study on the internal short circuit and failure mechanism of lithium-ion batteries under mechanical abuse conditions. Journal of Energy Storage, 89, 111819.

[26] Bhaskar, K., Kumar, A., Bunce, J., Pressman, J., Burkell, N., Miller, N., & Rahn, C. D. (2025). Short circuit detection in lithium-ion battery packs. Applied Energy, 380, 125087.

[27] Ge, S., Sasaki, T., Gupta, N., Qin, K., Longchamps, R. S., Aotani, K., ... & Wang, C. Y. (2024). Quantification of lithium battery fires in internal short circuit. ACS Energy Letters, 9(12), 5747-5755.

[28] Zhang, B., Chen, Z., Tao, Q., Jiao, M., Li, P., & Zhou, N. (2024). Characterization study on external short circuit for lithium-ion battery safety management: From single cell to module. Journal of Energy Storage, 99, 113239.

[29] Gao, R., Liang, H., Zhang, Y., Zhao, H., & Chen, Z. (2024). Characterization of lithium-ion batteries after suffering micro short circuit induced by mechanical stress abuse. Applied Energy, 374, 123931.

[30] Xu, W., Zhou, K., Wang, H., Lu, L., Wu, Y., Gao, B., ... & Li, Y. (2024). Series arc-induced internal short circuit leading to thermal runaway in lithium-ion battery. Energy, 308, 132999.

[31] Liu, X., Li, Y., Jiang, X., & Xu, K. (2024). Lithium-ion battery of an electric vehicle short circuit caused by electrolyte leakage: A case study and online detection. Journal of Energy Storage, 97, 112950.

[32] Qiao, D., Wei, X., Jiang, B., Fan, W., Lai, X., Zheng, Y., & Dai, H. (2024). Quantitative diagnosis of internal short circuit for lithium-ion batteries using relaxation voltage. IEEE Transactions on Industrial Electronics, 71(10), 13201-13210.

[33] Naresh, G., Praveenkumar, T., Madheswaran, D. K., Varuvel, E. G., Pugazhendhi, A., Thangamuthu, M., & Muthiya, S. J. (2025). Battery fault diagnosis methods for electric vehicle Lithium-ion batteries: Correlating codes and battery management system. Process Safety and Environmental Protection, 106919.

[34] Hong, J., Liang, F., Yang, J., & Du, S. (2024). An exhaustive review of battery faults and diagnostic techniques for real-world electric vehicle safety. Journal of Energy Storage, 99, 113234.

[35] Ji, H., Chung, Y. H., Pan, X. H., Hua, M., Shu, C. M., & Zhang, L. J. (2021). Study of lithium-ion battery module's external short circuit under different temperatures. Journal of Thermal Analysis & Calorimetry, 144(3).

[36] Xia, B., Chen, Z., Mi, C., & Robert, B. (2014, June). External short circuit fault diagnosis for lithium-ion batteries. In 2014 IEEE transportation electrification conference and expo (ITEC) (pp. 1-7). IEEE.

[37] Wang, G., Yang, J., & Jiao, J. (2022). Voltage correlation-based principal component analysis method for short circuit fault diagnosis of series battery pack. IEEE Transactions on Industrial Electronics, 70(9), 9025-9034.

[38] Sun, J., Lu, G., Shang, Y., Ren, S., & Wang, D. (2023). A minor-fault diagnosis approach based on modified variance for lithium-ion battery strings. Journal of Energy Storage, 63, 106965.

[39] Yu, Q., Wang, C., Li, J., Xiong, R., & Pecht, M. (2023). Challenges and outlook for lithium-ion battery fault diagnosis methods from the laboratory to real world applications. ETransportation, 17, 100254.

[40] Yang, Q., Sun, J., Kang, Y., Ma, H., & Duan, D. (2023). Internal short circuit detection and evaluation in battery packs based on transformation matrix and an improved state-space model. Energy, 276, 127555.

[41] Song, S., Tang, X., Sun, Y., Sun, J., Li, F., Chen, M., ... & Zhang, L. (2024). Fault evolution mechanism for lithium-ion battery energy storage system under multi-levels and multi-factors. Journal of Energy Storage, 80, 110226.

[42] Avinash, D. H., & Rammohan, A. (2023). A Comprehensive Review on Advanced Fault Detection Techniques of Lithium-ion Battery Packs in Electric Vehicle Applications. International Journal of Renewable Energy Research (IJRER), 13(2), 925-943.

[43] Zheng, Y., Shen, A., Han, X., & Ouyang, M. (2022). Quantitative short circuit identification for single lithium-ion cell applications based on charge and discharge capacity estimation. Journal of Power Sources, 517, 230716.

[44] Xu, Y., Ge, X., Shen, W., & Yang, R. (2022). A soft short-circuit diagnosis method for lithium-ion battery packs in electric vehicles. IEEE Transactions on Power Electronics, 37(7), 8572-8581.

[45] Lai, X., Jin, C., Yi, W., Han, X., Feng, X., Zheng, Y., & Ouyang, M. (2021). Mechanism, modeling, detection, and prevention of the internal short circuit in lithium-ion batteries: Recent advances and perspectives. Energy Storage Materials, 35, 470-499.

[46] Sarkar, S., Halim, S. Z., El-Halwagi, M. M., & Khan, F. I. (2022). Electrochemical models: methods and applications for safer lithium-ion battery operation. Journal of the Electrochemical Society, 169(10), 100501.

[47] Ma, R., Deng, Y., & Wang, X. (2023). Simplified electrochemical model assisted detection of the early-stage internal short circuit through battery aging. Journal of Energy Storage, 66, 107478.

[48] Zhao, J., Liu, M., Zhang, B., Wang, X., Liu, D., Wang, J., ... & Zhu, Y. (2023). Review of lithium-ion battery fault features, diagnosis methods, and diagnosis procedures. IEEE Internet of Things Journal, 11(11), 18936-18950.

[49] Chen, S., Sun, J., Tang, Y., & Zhang, F. (2024). A fault diagnosis method of battery internal short circuit based on multi-feature recognition. Transactions of the Institute of Measurement and Control, 46(11), 2186-2197.

[50] Zhang, Z., Gu, X., Mao, Z., Li, J., Li, X., & Shang, Y. (2024). A Rapid-Accurate Fault Diagnosis Method Based on Cumulative Probability Distribution for Lithium-Ion Battery Packs. IEEE Transactions on Industrial Electronics.

[51] Qiao, D., Wei, X., Fan, W., Jiang, B., Lai, X., Zheng, Y., ... & Dai, H. (2022). Toward safe carbon–neutral transportation: Battery internal short circuit diagnosis based on cloud data for electric vehicles. Applied Energy, 317, 119168.

[52] Sun, T., Zhu, H., Xu, Y., Jin, C., Zhu, G., Han, X., ... & Zheng, Y. (2024). Internal short circuit fault diagnosis for the lithium-ion batteries with unknown parameters based on transfer learning optimized residual network by multi-label data processing. Journal of Cleaner Production, 444, 141224.

[53] Shuhang, W., Ruoyu, W., Yuhao, W., Siwen, C., Shiyou, X., & Jinlei, S. (2024, October). Research on Internal Short-circuit Fault Diagnosis Based on Correlation Coefficient Method. In 2024 8th International Conference on Smart Grid and Smart Cities (ICSGSC) (pp. 159-163). IEEE.

[54] Qiao, D., Wang, X., Lai, X., Zheng, Y., Wei, X., & Dai, H. (2022). Online quantitative diagnosis of internal short circuit for lithium-ion batteries using incremental capacity method. Energy, 243, 123082.

[55] Wu, X., Wei, Z., Wen, T., Du, J., Sun, J., & Shtang, A. A. (2023). Research on short-circuit fault-diagnosis strategy of lithium-ion battery in an energy-storage system based on voltage cosine similarity. Journal of Energy Storage, 71, 108012.

[56] Li, C., Zeng, K., Li, B., Li, G., Yang, H., & Li, S. (2024). Internal short-circuit fault diagnosis for batteries of energy storage stations based on multivariate multiscale sample entropy. IEEE Transactions on Industrial Electronics.

[57] Jiang, J., Zhang, R., Wu, Y., Chang, C., & Jiang, Y. (2022). A fault diagnosis method for electric vehicle power lithium battery based on wavelet packet decomposition. Journal of Energy Storage, 56, 105909.

[58] Hamam, H. (2025). Rethinking Intelligence: From Human Cognition to Artificial Futures. Vokasi Unesa Bulletin of Engineering, Technology and Applied Science, 2(3), 531-548.

[59] Ajuji, M., Dawaki, M., Mohammed, A., & Ahmad, A. (2025). Estimating Residential Natural Gas Demand and Consumption: A Hybrid Ensemble Machine Learning Approach. Vokasi Unesa Bulletin of Engineering, Technology and Applied Science, 2(3), 549-557.

[60] Xu, C., Li, L., Xu, Y., Han, X., & Zheng, Y. (2022). A vehicle-cloud collaborative method for multi-type fault diagnosis of lithium-ion batteries. Etransportation, 12, 100172.

[61] Zhao, J., Feng, X., Pang, Q., Fowler, M., Lian, Y., Ouyang, M., & Burke, A. F. (2024). Battery safety: Machine learning-based prognostics. Progress in Energy and Combustion Science, 102, 101142.

[62] Zhang, J., Wang, Y., Jiang, B., He, H., Huang, S., Wang, C., ... & Ouyang, M. (2023). Realistic fault detection of li-ion battery via dynamical deep learning. Nature Communications, 14(1), 5940.

[63] Wang, G., Zhao, G., Xie, J., & Liu, K. (2023). Ensemble learning-based correlation coefficient method for robust diagnosis of voltage sensor and short-circuit faults in series battery packs. IEEE Transactions on Power Electronics, 38(7), 9143-9156.

[64] Li, J., Che, Y., Zhang, K., Liu, H., Zhuang, Y., Liu, C., & Hu, X. (2024). Efficient battery fault monitoring in electric vehicles: Advancing from detection to quantification. Energy, 313, 134150.

[65] Qiao, D., Wei, X., Jiang, B., Fan, W., Gong, H., Lai, X., ... & Dai, H. (2024). Data-driven fault diagnosis of internal short circuit for series-connected battery packs using partial voltage curves. IEEE Transactions on Industrial Informatics, 20(4), 6751-6761.

[66] Wei, Z., Liu, K., Liu, X., Li, Y., Du, L., & Gao, F. (2023). Multilevel data-driven battery management: From internal sensing to big data utilization. IEEE Transactions on Transportation Electrification, 9(4), 4805-4823.

[67] Zhang, Y., & Li, Y. F. (2022). Prognostics and health management of Lithium-ion battery using deep learning methods: A review. Renewable and sustainable energy reviews, 161, 112282.

[68] Cui, B., Wang, H., Li, R., Xiang, L., Du, J., Zhao, H., ... & Du, C. (2023). Internal short circuit early detection of lithium-ion batteries from impedance spectroscopy using deep learning. Journal of Power Sources, 563, 232824.

[69] Wang, L., Qiu, Y., Yuan, W., Tian, Y., & Zhou, Z. (2025). Next-generation battery safety management: machine learning assisted life-time prediction and performance enhancement. Journal of Energy Chemistry.

[70] Nozarijouybari, Z., & Fathy, H. K. (2024). Machine learning for battery systems applications: Progress, challenges, and opportunities. Journal of Power Sources, 601, 234272.

[71] Zhao, J., Feng, X., Pang, Q., Fowler, M., Lian, Y., Ouyang, M., & Burke, A. F. (2024). Battery safety: Machine learning-based prognostics. Progress in Energy and Combustion Science, 102, 101142.

[72] Fan, Z., Zi-xuan, X., & Ming-hu, W. (2022). Fault diagnosis method for lithium-ion batteries in electric vehicles using generalized dimensionless indicator and local outlier factor. Journal of Energy Storage, 52, 104963.

[73] Liu, H., Zhang, L., & Li, L. (2024). Progress on the fault diagnosis approach for lithium-ion battery systems: Advances, challenges, and prospects. Protection and Control of Modern Power Systems, 9(5), 16-41.

[74] Li, M., Cheng, F., Yang, J., Duodu, M. M., & Tu, H. (2024). A Fault Detection Method for Electric Vehicle Battery System Based on Bayesian Optimization SVDD Considering a Few Faulty Samples. Energy Engineering, 121(9).

[75] Ali, Z. M., Jurado, F., Gandoman, F. H., & Ćalasan, M. (2024). Advancements in battery thermal management for electric vehicles: Types, technologies, and control strategies including deep learning methods. Ain Shams Engineering Journal, 15(9), 102908.

[76] Li, H. S., Fan, P., Peng, H., Song, S., & Long, G. L. (2021). Multilevel 2-d quantum wavelet transforms. IEEE Transactions on Cybernetics, 52(8), 8467-8480.

[77] Cheng, F., Li, M., Tu, H., Bennaceur, A., & Wen, Y. (2025). A novel fault detection and isolation method for electric vehicle introducing kernel differential of SVDD. Journal of Energy Storage, 123, 116660.

[78] Huang, X., Zhang, F., Fan, H., Chang, H., Zhou, B., & Li, Z. (2024). Pseudo anomalies enhanced deep support vector data description for electrocardiogram quality assessment. Computers in Biology and Medicine, 170, 107928.

[79] Gu, X., Li, J., Liu, K., Zhu, Y., Tao, X., & Shang, Y. (2023). A precise minor-fault diagnosis method for lithium-ion batteries based on phase plane sample entropy. IEEE Transactions on Industrial Electronics, 71(8), 8853-8861.